

# SENSEI: Characterization of Single-Electron Events Using a Skipper-CCD

The SENSEI Collaboration:

Liron Barak,<sup>1</sup> Itay M. Bloch,<sup>1</sup> Ana Botti,<sup>2,3</sup> Mariano Cababie,<sup>2,3,\*</sup> Gustavo Cancelo,<sup>3</sup> Luke Chaplinsky,<sup>4,5</sup> Fernando Chierchie,<sup>3</sup> Michael Crisler,<sup>3</sup> Alex Drlica-Wagner,<sup>3,6,7</sup> Rouven Essig,<sup>4</sup> Juan Estrada,<sup>3</sup> Erez Etzion,<sup>1</sup> Guillermo Fernandez Moroni,<sup>3</sup> Daniel Gift,<sup>4,5</sup> Stephen E. Holland,<sup>8</sup> Sravan Munagavalasa,<sup>4,5</sup> Aviv Orly,<sup>1</sup> Dario Rodrigues,<sup>2,3</sup> Aman Singal,<sup>5</sup> Miguel Sofo Haro,<sup>3,9</sup> Leandro Stefanazzi,<sup>3</sup> Javier Tiffenberg,<sup>3</sup> Sho Uemura,<sup>1</sup> Tomer Volansky,<sup>1</sup> and Tien-Tien Yu<sup>10</sup>

<sup>1</sup>*School of Physics and Astronomy, Tel-Aviv University, Tel-Aviv 69978, Israel*

<sup>2</sup>*Department of Physics, FCEN, University of Buenos Aires and IFIBA, CONICET, Buenos Aires, Argentina*

<sup>3</sup>*Fermi National Accelerator Laboratory, PO Box 500, Batavia IL, 60510, USA*

<sup>4</sup>*C.N. Yang Institute for Theoretical Physics,*

*Stony Brook University, Stony Brook, NY 11794, USA*

<sup>5</sup>*Department of Physics and Astronomy, Stony Brook University, Stony Brook, NY 11794, USA*

<sup>6</sup>*Kavli Institute for Cosmological Physics, University of Chicago, Chicago, IL 60637, USA*

<sup>7</sup>*Department of Astronomy and Astrophysics,*

*University of Chicago, Chicago IL 60637, USA*

<sup>8</sup>*Lawrence Berkeley National Laboratory, One Cyclotron Road, Berkeley, California 94720, USA*

<sup>9</sup>*Centro Atómico Bariloche, CNEA/CONICET/IB, Bariloche, Argentina*

<sup>10</sup>*Department of Physics and Institute for Fundamental Science,*

*University of Oregon, Eugene, Oregon 97403, USA*

(Dated: October 22, 2021)

We use a science-grade Skipper Charge Coupled Device (Skipper-CCD) operating in a low-radiation background environment to develop a semi-empirical model that characterizes the origin of single-electron events in CCDs. We identify, separate, and quantify three independent contributions to the single-electron events, which were previously bundled together and classified as “dark counts”: dark current, amplifier light, and spurious charge. We measure a dark current, which depends on exposure, of  $(5.89 \pm 0.77) \times 10^{-4} e^-/\text{pix}/\text{day}$ , and an unprecedentedly low spurious charge contribution of  $(1.52 \pm 0.07) \times 10^{-4} e^-/\text{pix}$ , which is exposure-independent. In addition, we provide a technique to study events produced by light emitted from the amplifier, which allows the detector’s operation to be optimized to minimize this effect to a level below the dark-current contribution. Our accurate characterization of the single-electron events allows one to greatly extend the sensitivity of experiments searching for dark matter or coherent neutrino scattering. Moreover, an accurate understanding of the origin of single-electron events is critical to further progress in ongoing R&D efforts of Skipper and conventional CCDs.

## INTRODUCTION

Charged coupled devices (CCDs) are widely used photon detectors for scientific purposes since their invention in 1969 [1, 2]. More recently, they have also been adopted as particle detectors in rare-event searches for coherent neutrino scattering [3] and dark matter particles [4, 5]. The development of the Skipper-CCD [6], with its deep sub-electron read-out noise and resulting ability to detect events producing only a single photon or a single electron, has revolutionized the search for coherent neutrino scattering and dark matter particles, since these produce events typically containing only one or a few ionized electrons [7, 8]. The first science results from data collected with a single Skipper-CCD have already been presented in [9–11], and the construction of large-mass detectors for both neutrino and dark matter particles searches is underway or planned [11–14].

The data from [9–11] contains a large number of single-electron events (SEE). A detailed understanding of the

nature and origin of these SEE in silicon crystals, and in (Skipper-)CCDs in particular, is crucial both for maximizing the sensitivity to coherent neutrino scattering and to dark matter and for assessing the discovery potential of these experiments.

We present in this paper a new set of techniques to identify and characterize the nature and origin of SEE utilizing a science-grade Skipper-CCD. We employ a Skipper-CCD from the first batch of sensors fabricated using ultra high-resistivity silicon ( $R > 18 \text{ k}\Omega$ ). We also propose a semi-empirical model that describes the observed SEE. The methodology described here provides a set of techniques that we expect can be implemented with any Skipper-CCDs. Furthermore, it enables current and planned experiments utilizing Skipper-CCDs, such as CONNIE, SENSEI, DAMIC-M, and Oscura, to mitigate these background events and greatly enhance their sensitivity to, and discovery potential of, coherent neutrino scattering and sub-GeV dark matter.

## TECHNICAL DESCRIPTION

We provide here a brief description of the Skipper-CCD and the data taking.

### The Skipper-CCD

The measurements presented in this work were performed using a science-grade Skipper-CCD from the SENSEI experiment [11]. The sensors were designed by the Lawrence Berkeley National Laboratory (LBNL), and fabricated at Teledyne/DALSA using high-resistivity ( $>18\text{k}\Omega\text{-cm}$ ) silicon wafers with a thickness of  $675\ \mu\text{m}$ . The packaging and testing of the sensors was done at the SiDet facility at the Fermi National Accelerator Laboratory (FNAL) using the package design described in [11]. The sensor was installed in a vacuum vessel that was placed in a low-radiation environment at the MINOS underground facility at FNAL. The shielding surrounding the Skipper-CCD can be divided into an “internal” and an “external” shield, corresponding to whether it was installed inside or outside of the vacuum vessel that houses the Skipper-CCD. During the course of the measurements the external shielding was installed. For details on both types of shielding see [11].

The Skipper-CCD used for this work has four identical readout stages, one in each corner. The usual mode of operation is to read out one quarter (a quadrant) of the Skipper-CCD through the corresponding sensor, simultaneously and independently of the readout of the other quadrants. However, there are no physical barriers between the quadrants and it is possible to read the entire Skipper-CCD though any one of the readout stages if desired. The active area is a standard LBNL three-phase CCD with a buried  $p$ -channel fabricated on a high-resistivity  $n$ -type bulk. Each column of pixels is separated by “channel stops”, highly doped regions that prevent the spread of the charges from one column into another. The fabrication process for this detector was optimized for dark matter searches, and no polishing of the backside (usually referred to as “thinning”) was done

	Value	Units
CCD dimensions	$6144 \times 886$	pixels
Pixel Size	$15 \times 15$	$\mu\text{m}^2$
Thickness	675	$\mu\text{m}$
Total mass	1.926	g
CCD temperature	135	K
Number of amplifiers	4 (2 used)	
Readout time (1 sample)	42.825	$\mu\text{s}$
Readout noise (1 sample)	2.5	$e^-$ rms / pix
Readout noise (n samples)	$\frac{2.5}{\sqrt{n}}$	$e^-$ rms / pix

TABLE I. Main characteristics of the Skipper-CCD used in this work.

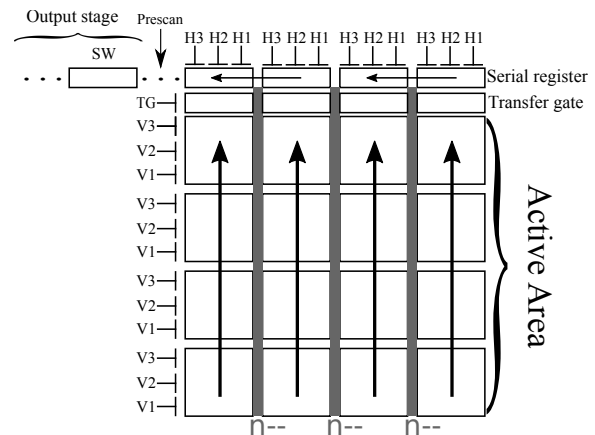


FIG. 1. Schematic illustration of a  $4 \times 4$  pixels quadrant of a CCD. The arrows show the direction in which collected charges are transferred during readout. A detailed schematic of the readout stage is provided in Fig. 2. H1, H2 and H3 are the last horizontal clocks in the serial register before the Summing Well (SW). In gray, highly doped  $n$ -type “channel stops”.

to preserve as much target mass as possible. The silicon bulk is fully depleted at approximately 40 V but was operated at a 70 V substrate voltage to reduce the diffusion of charge to neighboring pixels in the bulk.

The detector was operated at low temperature (135 K) to reduce the probability of surface and bulk electrons to be promoted into the conduction band due to thermal agitation [2]. At this temperature, the fraction of thermally-induced events, which we refer to as “intrinsic dark current”, is sub-dominant compared to other sources of charge [11]. Operating the sensor at even lower temperatures had the undesirable effect of increasing the charge transfer inefficiency. As there was an unusual excess of SEE in the third quadrant and a high charge transfer inefficiency in the fourth quadrant, the data collected by these two quadrants was not used in the final analysis. A brief summary of the Skipper-CCD’s characteristics is given in Table I.

As shown in Fig. 1, each quadrant of the CCD can be divided into four regions: active area, transfer gate, serial register, and readout stage. The active area of each quadrant is an array of  $3072 \times 443$  pixels where the charges are collected during the exposure of the CCD sensor. A schematic depiction of the readout stage is provided in Fig. 2.

### Data-taking cycle

The standard data-taking cycle of a CCD consists of three phases:

- **Cleaning.** During this phase, the substrate bias of the CCD is set at 0 V whereas the voltage on the

surface of the CCD is set sufficiently high in order to fill traps on the surface with holes from the channel stops [15], thereby reducing intrinsic dark current and “resetting” the CCD. At the end of this procedure, the substrate voltage is set back to the depletion voltage and the surface clocks are set to their previous configuration. The entire CCD is then read out in order to remove all of the accumulated charge so that one can start the next phase with a “clean” CCD.

- **Exposure.** During this phase all voltages are kept fixed. Any ionizing interaction that occurs within the active area of the detector therefore leaves electrons trapped inside the pixels, which are later read during the readout phase.  $V_{DD}$ , the bias voltage for the output transistor M1, is set to 0 during this phase and turned on during the other phases.
- **Readout.** The collected charges are transferred vertically row by row into the serial register through the transfer gate. Once the charges reach the serial register, they are transported horizontally, one pixel at a time, to the readout stage (Fig. 1). At the readout stage, the charges collected in each pixel are converted into a voltage signal that is finally measured by the readout electronics (Fig. 2).

### SEMI-EMPIRICAL MODEL FOR THE ORIGIN OF THE SINGLE-ELECTRON EVENTS

The SEE per pixel have two main contributions that scale with time: events produced during Exposure ( $\mu_{EXP}$ ) and events produced during Readout ( $\mu_{RO}$ ). The rates of these contributions are expected to be different as the amount of light produced by the readout stage depends on the base current of the output transistor, which varies during Readout and is turned off during the Exposure phase under normal operating conditions. We identify also a time-independent contribution, which we define as spurious charge ( $\mu_{SC}$ ). Spurious charge is generated during the clocking of the active area and serial register. Such events are produced during the Cleaning and

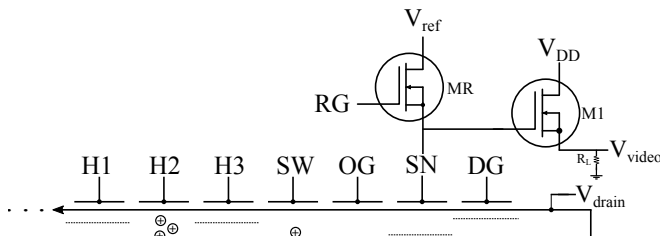


FIG. 2. Schematic illustration of a Skipper-CCD readout stage. H1, H2 and H3 are the last horizontal clocks in the serial register before the Summing Well (SW).

Readout phases and will be discussed later on. Since they depend solely on the number of times a pixel is clocked (*i.e.*, the number of times a pixel transfers charges to its neighbor), they are modeled as an additional exposure-independent term.

Following these definitions, the total number ( $\mu$ ) of SEE per pixel generated during a data-taking cycle can be written as

$$\begin{aligned} \mu(t_{EXP}, t_{RO}) &= \mu_{EXP}(t_{EXP}) + \mu_{RO}(t_{RO}) + \mu_{SC} \\ &= \lambda_{EXP}t_{EXP} + \lambda_{RO}t_{RO} + \mu_{SC}, \end{aligned} \quad (1)$$

where in the second line we assumed that both  $\mu_{EXP}$  and  $\mu_{RO}$  scale linearly with time. The parameters  $\lambda_{EXP}$  and  $\lambda_{RO}$  are the SEE rates during exposure and readout phase, respectively, in units of events per pixel per day, while the times  $t_{EXP}$  and  $t_{RO}$  are expressed in days.

There are three contributions to the SEE: dark current, amplifier light, and spurious charge. In the following subsection we discuss each of these contributions in detail. In that discussion, these contributions will be classified based on the following primary characteristics: spatial distribution (localized or uniform) and time-dependence. Throughout our analysis we use the event-selection criteria discussed in [11] and summarized in Table I of that paper, with the exception of the edge mask and the halo mask (cuts number 6 and 9 of Table I of [11]), which we set to 40 pixels (instead of 60) to increase the statistics for this work.

### Dark current

Although the CCD is inside a sealed vacuum vessel, SEE can be generated in the CCD during Exposure in the absence of any external source (except unavoidable environmental radiation) and not because charges are shifted from pixel-to-pixel (as would occur during readout). We refer to SEE generated in this way as dark current (DC) and differentiate between two distinct contributions: intrinsic and extrinsic, depending on whether the current is generated by the CCD itself (intrinsic) or through an interaction with its environment (extrinsic). DC contributes during both the Exposure and Readout phases of data-taking. The number of events coming from DC scales linearly with time during the Exposure phase and hence  $\lambda_{DC}$  will be one of the components of  $\lambda_{EXP}$ . During the Readout phase, the exposure of the pixels is non-uniform as the last pixel read has an additional exposure time of  $t_{RO}$  when compared to the pixel that is read first. Overall, the average contribution of the DC during the Readout phase is given by  $\lambda_{DC}/2$ .

### *Intrinsic dark current*

Intrinsic dark current (usually referred plainly as dark current in the literature) is the most well-studied current contribution for SEE [2, 16]. This source generates, via thermal fluctuations across the silicon band-gap, single electron-hole pairs. The holes, which we collect using a  $p$ -buried channel, are trapped in the potential wells within the pixels. Since this thermal agitation is a random process independent of time and space, the number of holes collected from the thermal agitation in a pixel for a given period of time is a random variable that follows a Poisson distribution. The expected value is the intrinsic DC rate multiplied by the exposure time of the pixel. We can further differentiate between two types of intrinsic DC that appear in a buried-channel CCD: bulk and surface intrinsic DC. The latter component can be greatly reduced, at least temporarily, with an inversion of the surface in the Cleaning phase [15]. This empties the traps that mediate the generation of surface DC. The traps begin to fill again during the subsequent Exposure phase, but this recovery is inhibited at low temperature. Estimates from the model developed in [17] show that less than 0.1% of the surface intrinsic DC is recovered at the operating temperature of 135 K after 24 hours (much longer than any measurement carried out during this work). Therefore, we find that the bulk component dominates the intrinsic DC.

### *Extrinsic dark current*

In [11], we reported a SEE rate of  $(1.594 \pm 0.160) \times 10^{-4} e^-/\text{pix}/\text{day}$ , which, despite being the lowest value ever reported in a CCD, is at least one order of magnitude above the theoretically expected intrinsic DC rate at 135 K. This discrepancy is explained by additional environmentally-induced contributions to the observed SEE, distributed approximately uniformly across the CCD (after applying the event-selection criteria and with the given statistical uncertainties) and, as the intrinsic DC, increasing linearly with the exposure time. In this sense it is, in principle, indistinguishable from the intrinsic DC. This extrinsic contribution was identified for the first time in [11] and is directly related to the environmental radiation. A detailed discussion of the physical processes that likely explain these SEE is discussed in [18].

### **SEE produced by amplifier light**

As the number of SEE per pixel decreases with lower temperature and background radiation as well as improved detector performance, new low-energy signals appear that are not contained in the definition of DC. This

collaboration recently reported an excess of SEE near the readout stage [10], which we refer to as amplifier-light events. This effect was previously investigated by many authors [19–23] and is due to infrared photons emitted by the M1 transistor of the readout stage (see Fig 2). Because the photons have a finite range in silicon and are emitted continuously, charge generated by this effect is spatially localized in the region near the readout stage and increases linearly with time. We express the corresponding rate as  $\lambda_{\text{AL}}$  (in units of events per pixel per day). As this contribution is localized,  $\lambda_{\text{AL}}$  depends not only on the distance from the readout stage but on which zone of the CCD is under study. For the sake of simplicity, we average  $\lambda_{\text{AL}}$  over the whole CCD and do not study the spatial dependence.

Since  $V_{\text{DD}}$  is set to 0 during Exposure, SEE due to amplifier light are only produced in Readout and Cleaning phases. Note that if  $V_{\text{DD}}$  is kept on during the Exposure phase, an additional non-negligible amplifier light contribution must be taken into account. That contribution may be different, since the voltage in the floating gate (which is also the gate of the M1 transistor, see Fig. 2) is constant during Exposure but changes rapidly during Readout. Moreover, as the active area is being read and pixels are being transported to the sense node, the spatial dependence of the amplifier light during the Readout and Exposure phases is different.

### **Spurious charge**

The last SEE contribution to take into consideration is the spurious charge (SC), which is generated when the voltages in the active area or serial register are clocked [2, 24, 25]. As noted earlier, SCs are generated during both Cleaning and Readout phases and depend solely on the number of times a pixel is clocked. Therefore, the SC is a spatially uniform, time-independent, intrinsic contribution to the SEE.

### **Empirical model**

Given the three contributions discussed in the previous sections, we can express both  $\lambda_{\text{EXP}}$  and  $\lambda_{\text{RO}}$  as follows

$$\lambda_{\text{EXP}} = \lambda_{\text{DC}}, \quad (2)$$

$$\lambda_{\text{RO}} = \frac{\lambda_{\text{DC}}}{2} + \lambda_{\text{AL}}, \quad (3)$$

Contribution ( $e^-/\text{pix}$ )		Time dependence			Spatial distribution
		Linear		Independent	
		Exposure	Readout		
Dark current	Intrinsic	$\lambda_{\text{DC}} t_{\text{EXP}}$	$\frac{\lambda_{\text{DC}}}{2} t_{\text{RO}}$	-	Uniform
	Extrinsic				Uniform
Amplifier-light current		-	$\lambda_{\text{AL}} t_{\text{RO}}$	-	Localized
Spurious charge		-	-	$\mu_{\text{SC}}$	Uniform

TABLE II. Summary of charge contributions and their properties, following Eq. 4. The units for  $\lambda_{\text{DC}}$  and  $\lambda_{\text{AL}}$  are  $e^-/\text{pix}/\text{day}$ , while  $\mu_{\text{SC}}$  is in  $e^-/\text{pix}$ . At 135 K and after an inversion of the CCD surface, the intrinsic DC is dominated by the bulk intrinsic DC, which has a clear linear time-dependence; we can ignore the surface intrinsic DC which has a non-linear time-dependence.

and re-write Eq. (1) to obtain our full empirical model:

$$\begin{aligned} \mu(t_{\text{EXP}}, t_{\text{RO}}) &= \lambda_{\text{DC}} t_{\text{EXP}} \\ &+ \left( \frac{\lambda_{\text{DC}}}{2} + \lambda_{\text{AL}} \right) t_{\text{RO}} \\ &+ \mu_{\text{SC}}. \end{aligned} \quad (4)$$

A summary of the charge contributions that enter Eq. (4) can be found in Table II. In the next section, we use this model to characterize SEE in a SENSEI Skipper-CCD.

### SINGLE-ELECTRON EVENTS TRANSFER CURVES

Using the model in Eq. (4), we propose a new set of methods to measure  $\lambda_{\text{DC}}$ ,  $\lambda_{\text{AL}}$ , and  $\mu_{\text{SC}}$ . These techniques provide the “transfer curves” for SEE as a function of both exposure and readout time. We use two techniques to measure all of the parameters in Eq. (4):

**I. Determination of  $\lambda_{\text{DC}}$ .** We record several images with a range of different exposure times and a fixed readout time. For each image (with a given exposure time), we measure the amount of SEE per pixel. We then plot the SEE per pixel as a function of the exposure time and perform a linear fit. The slope of this linear function corresponds to  $\lambda_{\text{DC}}$  as shown in Eq. (5), and the  $y$ -intercept is the SEE rate from the readout ( $\mu_{\text{RO}}$  for a fixed readout time  $t_{\text{RO}}$ ) plus the SC ( $\mu_{\text{SC}}$ ):

$$\mu(t_{\text{EXP}}) = \lambda_{\text{DC}} t_{\text{EXP}} + (\mu_{\text{RO}} + \mu_{\text{SC}}). \quad (5)$$

**II. Determination of  $\lambda_{\text{AL}}$  and  $\mu_{\text{SC}}$ .** Using the measured value for  $\lambda_{\text{DC}}$  obtained by the previous procedure,  $\lambda_{\text{AL}}$  and  $\mu_{\text{SC}}$  can be measured by taking multiple images with different readout times and zero exposure time. To avoid changing the geometry of

the active area (and hence the value of  $\lambda_{\text{AL}}$ ),  $t_{\text{RO}}$  is varied by changing the number of samples that are taken per pixel. For each image (with a given readout time), we measure the amount of SEE per pixel. We then plot the SEE as a function of  $t_{\text{RO}}$  and perform a linear fit. The slope of this linear function is  $\frac{\lambda_{\text{DC}}}{2} + \lambda_{\text{AL}}$  as shown in Eq. (6), while the  $y$ -intercept is  $\mu_{\text{SC}}$ :

$$\mu(t_{\text{RO}}) = \left( \frac{\lambda_{\text{DC}}}{2} + \lambda_{\text{AL}} \right) t_{\text{RO}} + \mu_{\text{SC}}. \quad (6)$$

### RESULTS AND DISCUSSION

We study four datasets (see Table III):

- A:** To determine  $\lambda_{\text{DC}}$ , eight images were taken, each with a different exposure time  $t_{\text{EXP}}$  but the same readout time  $t_{\text{RO}}$ .
- B:** To study the amplifier light contribution, nine datasets were analyzed, each consisting of six zero-exposure images; each set consists of a different  $V_{\text{DD}}$  voltage value applied in the M1 transistor (see Fig. 2), scanning from  $-17$  V to  $-25$  V in 1 V steps.
- C&D:** To measure  $\mu_{\text{SC}}$  and  $\lambda_{\text{AL}}$ , seven datasets were used, each consisting of two zero-exposure images and a different readout time  $t_{\text{RO}}$ . We use two different experimental configurations: for the first (dataset C) we set  $V_{\text{DD}}$  at  $-22$  V while avoiding the use of an external shield (same as dataset A). For the second (dataset D) we set the  $V_{\text{DD}}$  at  $-21$  V and add an additional external shield (see discussion in the Technical Description section).

As mentioned before, the same event-selection criteria shown in Table I of [11] is used, except that the edge and halo mask are set to 40 pixels (instead of 60 pixels) in order to increase statistics (see Fig. 3).

	A	B	C	D
Skipper samples	250	250	200-950	200-950
$V_{DD}$ voltage (-V)	22	17-25	22	21
External shield	No	Yes	No	Yes
Exposure time (hs)	0-8	0	0	0
Readout time (h:m:s)	4:57:00	0:55:43	Variable	Variable

TABLE III. Description of each dataset in the section analysis specifying skipper samples (number of samples measured for a given pixel),  $V_{DD}$  voltage (voltage applied to the M1 transistor drain channel as shown in Fig. 2), external lead shield presence and both exposure and readout time. These last two, as also the number of skipper samples, vary from image to image in the same dataset as explained in the text.

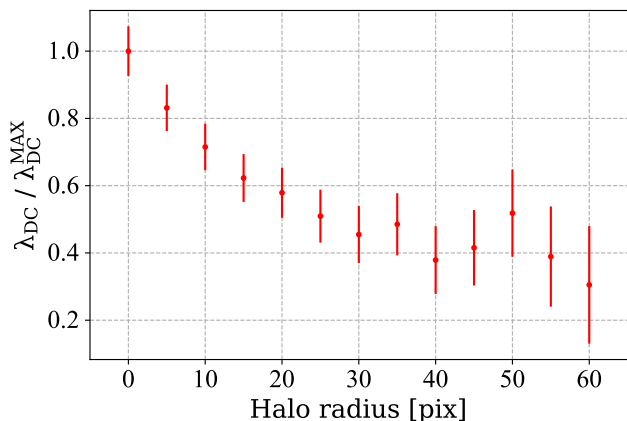


FIG. 3. The normalized dark current rate,  $\lambda_{DC}$ , as a function of the halo radius mask. As can be seen,  $\lambda_{DC}$  monotonically decreases until a halo radius of roughly 30 pixels. Dataset A was used for this figure.

#### Dark current

Using dataset A, we extract the number of SEE per pixel for each image and perform a linear regression using Eq. (5), taking the exposure time of each image  $t_{EXP}$  as the independent variable. As shown in Fig. 4, we obtain a DC rate of  $\lambda_{DC} = (5.89 \pm 0.77) \times 10^{-4} e^-/\text{pix}/\text{day}$ . This value is compatible with the  $(5.312^{+1.490}_{-1.277}) \times 10^{-4} e^-/\text{pix}/\text{day}$  reported in [11] for the configuration without the external shield.

Our measurement identifies a non-negligible value of the time-independent term ( $\mu_{RO} + \mu_{SC}$ ) (see Eq. (5)). This contribution dominates the number of SEE for exposures shorter than 15 hours. To trace its origin and to disentangle the contributions from  $\mu_{RO}$  and  $\mu_{SC}$ , we perform a dedicated study to understand the SEE produced by luminescence of the output transistor. Light generated in the readout stage can reach the pixels in

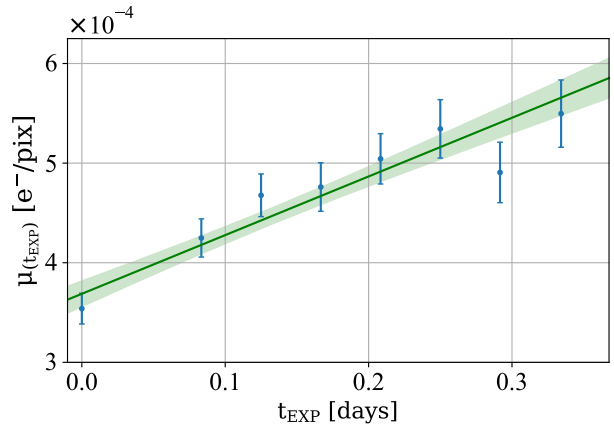


FIG. 4. Determination of  $\lambda_{DC}$ . SEE rate as a function of the exposure time  $t_{EXP}$  (**blue dots**). The linear regression of these measurements together with a  $1\sigma$  CL band is shown in **green**. The slope is found to be  $(5.89 \pm 0.77) \times 10^{-4} e^- \text{rms}/\text{pix}/\text{day}$  and the  $y$ -intercept  $(3.69 \pm 0.13) \times 10^{-4} e^-/\text{pix}$ . Dataset A was used for this figure.

the serial register and active area of the CCD during Readout and produce SEE that are independent of the exposure time. The next subsection discusses this characterization effort and how it leads to the optimization of the operation parameters.

#### Optimization of the operation parameters

To characterize the amplifier light contribution, we study the impact on the amplifier light events from varying the voltages in the readout stage. We focus on the voltage applied to the  $V_{DD}$  gate, which controls the drain voltage of the output transistor M1 (see Fig. 2), as previous works [20, 21] have shown that an increase in the current between the drain and source leads to an increase in light emission; this phenomenon is explained in the literature as bremsstrahlung radiation produced by hot electrons. These are electrons that, because of very localized high electric fields in the M1 transistor, make a transition from the valence to the conduction band, enabling photon emission as explained in [20].

To measure the amplifier light contribution we take zero-exposure images for nine different  $V_{DD}$  values (dataset B) to check if it impacts  $\mu_{RO}$ . As discussed at the end of the previous subsection, light emitted by the output transistor can produce SEE during Readout with a number that is independent of the exposure time. By taking zero-exposure images we are able to measure  $(\mu_{RO} + \mu_{SC})$  as a function of  $V_{DD}$ . The SC is not affected by  $V_{DD}$  as, by definition, it consists of charges that are produced due to the clocking of the pixels, serial register, and readout stage. Different values of  $V_{DD}$  will impact

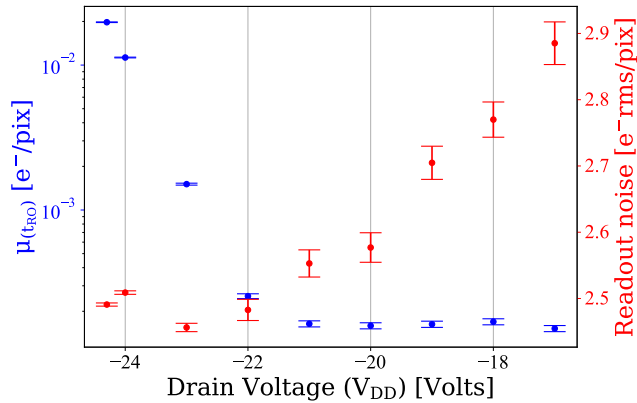


FIG. 5. Single-electron events (SEE) per pixel (blue, left axis) and single-sample readout noise (red, right axis) as a function of the drain voltage of the M1 transistor ( $V_{DD}$ ). Images are taken from dataset B.

$V_{DD}$	External Shield	$\lambda_{DC}$	$\lambda_{AL}$	$\mu_{SC}$
-21	Yes	$(1.59 \pm 0.16)$	$(0.36 \pm 0.18)$	$(1.52 \pm 0.07)$
-22	No	$(5.89 \pm 0.77)$	$(19.91 \pm 1.26)$	$(1.59 \pm 0.12)$

TABLE IV. Summary of charge contributions and results for  $V_{DD} = -21$  V and  $-22$  V. The units for  $\lambda_{DC}$  and  $\lambda_{AL}$  are  $10^{-4} e^-/\text{pix}/\text{day}$ , while  $\mu_{SC}$  is in  $10^{-4} e^-/\text{pix}$ .

$\mu_{RO}$  by producing changes in  $\lambda_{AL}$  (Eq. (6)).

In Fig. 5, we show the number of SEE per pixel for each of the 9 sets of images of dataset B as a function of  $V_{DD}$ . The number of SEE drastically decreases between  $-24$  V and  $-21$  V and reaches a plateau above  $-21$  V. This behavior is due to an increase of light emission in M1 as it is driven from its linear region (above  $-21$  V) to its saturation region. At the same time, a reduction of the  $V_{DD}$  value produces an increase on the electronic readout noise, which reduces the signal-to-noise ratio. Our technique allows one to optimize the operating conditions depending on the application.

The fact that the amount SEE in Fig. 5 is constant for values of  $V_{DD}$  above  $-21$  V suggests that only a small fraction of the total observed SEE are created from infrared photons emitted in the readout stage under these conditions. The leading contributions to SEE in this regime are expected to be the SC and DC collected during Readout.

To quantify the amount of amplifier light events produced during Readout ( $\lambda_{AL}$ ) when operating at  $-21$  V and  $-22$  V at  $V_{DD}$ , we take two sets of images with different  $t_{RO}$  (datasets C and D). These data also allow us to measure the amount of SC events under these conditions.

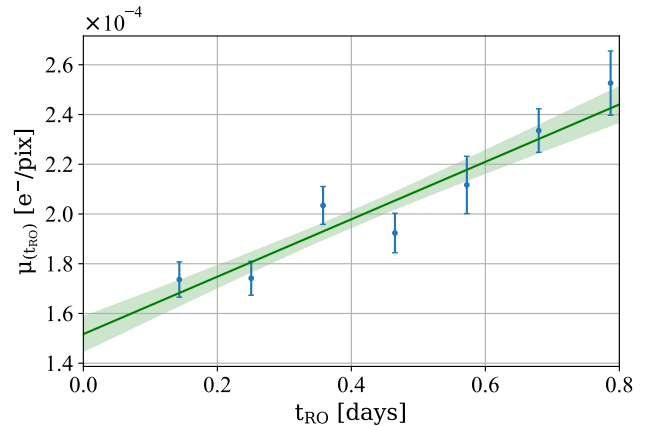


FIG. 6. Determination of  $\lambda_{AL}$  and  $\mu_{SC}$ . Extracted SEE rate versus readout time  $t_{RO}$  (blue dots) for images in dataset D. In green, the performed linear regression together with a  $1\sigma$  CL band in light green. The extracted value for the slope of the regression is  $(1.15 \pm 0.16) \times 10^{-4} e^-/\text{pix}/\text{day}$  and the  $y$ -intercept  $(1.52 \pm 0.07) \times 10^{-4} e^-/\text{pix}$ .

#### *Spurious charge and amplifier-light contribution*

To measure the parameters in Eq. (6), the following procedure was applied on both datasets C and D: the amount of SEE per pixel is extracted for each group of images with equal  $t_{RO}$  and a linear regression is performed. Fig. 6 illustrates this result for dataset D. Following Eq. (6), the slope of the regression is the sum of  $\lambda_{DC}/2$  and  $\lambda_{AL}$ , and the  $y$ -intercept is the amount of SC ( $\mu_{SC}$ ). For  $V_{DD} = -22$  V, and using the value for  $\lambda_{DC}$  obtained from dataset A,  $\lambda_{AL}$  is determined to be  $(19.91 \pm 1.26) \times 10^{-4} e^-/\text{pix}/\text{day}$ . For  $V_{DD} = -21$  V (the configuration used in [11]), we use the reported  $\lambda_{DC}$  from that work,  $(1.59 \pm 0.16) \times 10^{-4} e^-/\text{pix}/\text{day}$ , as a reference value for  $\lambda_{DC}$ .

Table IV summarizes the results after combining Eq. (6) and the values obtained from the linear regression for  $V_{DD} = -21$  V and  $V_{DD} = -22$  V. As shown, the optimization of the  $V_{DD}$  voltage from  $-22$  V to  $-21$  V reduces the number of amplifier light events by two orders of magnitude. Additionally, the  $y$ -intercept values ( $\mu_{SC}$ ) for both datasets C and D are compatible and do not depend on  $V_{DD}$ , or on the additional shielding, as expected. The development of methods to reduce the SC through the shaping of the clock profiles are ongoing.

## Conclusions

A new era of sub-electron noise CCDs has commenced. In this work, we provide an empirical model together with the tools to identify and measure the main contributions to single electron events (SEE) in Skipper-CCD sensors.

Using these techniques, we are able to identify, disentangle, and quantify individual contributions to the SEE rate previously grouped under the label “dark counts.” Our results determine three types of rates: the dark current (DC), a current of single events produced by amplifier light (AL), and the spurious charge (SC). In addition, by studying the dependence of the amplifier light on the drain voltage of the output transistor, we reduced this contribution by two orders of magnitude. The empirical modeling and techniques presented in this work provide a tool to optimize the operating conditions and push forward the capability of dark matter experiments based on the Skipper-CCD technology.

**ACKNOWLEDGMENTS.** We are grateful for the support of the Heising-Simons Foundation under Grant No. 79921. This work was supported by Fermilab under DOE Contract No. DE-AC02-07CH11359. The CCD development work was supported in part by the Director, Office of Science, of the DOE under No. DE-AC02-05CH11231. RE acknowledges support from DoE Grant DE-SC0009854, Simons Investigator in Physics Award 623940, and the US-Israel Binational Science Foundation Grant No. 2016153. The work of DG was supported in part by DoE Grant DE-SC0009854 and BSF grant No. 2016153. TV is supported by the Israel Science Foundation-NSFC (grant No. 2522/17), by the Binational Science Foundation (grant No. 2016153) and by the European Research Council (ERC) under the EU Horizon 2020 Programme (ERC-CoG-2015 - Proposal n. 682676 LDMThExp). The work of SU is supported in part by the Zuckerman STEM Leadership Program. IB is grateful for the support of the Alexander Zaks Scholarship, The Buchmann Scholarship, and the Azrieli Foundation. This manuscript has been authored by Fermi Research Alliance, LLC under Contract No. DE-AC02-07CH11359 with the U.S. Department of Energy, Office of Science, Office of High Energy Physics. The United States Government retains and the publisher, by accepting the article for publication, acknowledges that the United States Government retains a non-exclusive, paid-up, irrevocable, world-wide license to publish or reproduce the published form of this manuscript, or allow others to do so, for United States Government purposes.

---

\* mcababie@df.uba.ar

- [1] G. E. Smith, *Rev. Mod. Phys.* **82**, 2307 (2010).
- [2] J. Janesick, *Scientific charge-coupled devices*, Bellingham, WA: SPIE Optical Engineering Press, 2001, xvi, 906 p. SPIE Press monograph, PM 83. ISBN 0819436984 **83** (2001), 10.1117/12.7974139.
- [3] A. Aguilar-Arevalo, X. Bertou, C. Bonifazi, G. Canelo, A. Castañeda, B. Cervantes Vergara, C. Chavez, J. C. D’Olivo, J. a. C. dos Anjos, J. Estrada, A. R. Fernandez Neto, G. Fernandez Moroni, A. Foguel, R. Ford, J. Gonzalez Cuevas, P. Hernández, S. Hernandez, F. Izraelevitch, A. R. Kavner, B. Kilminster, K. Kuk, H. P. Lima, M. Makler, J. Molina, P. Mota, I. Nasteva, E. E. Paolini, C. Romero, Y. Sarkis, M. Sofu Haro, I. a. M. S. Souza, J. Tiffenberg, and S. Wagner (CONNIE Collaboration), *Phys. Rev. D* **100**, 092005 (2019).
- [4] J. Barreto *et al.* (DAMIC), *Phys. Lett. B* **711**, 264 (2012), arXiv:1105.5191 [astro-ph.IM].
- [5] A. Aguilar-Arevalo, D. Amidei, D. Baxter, G. Canelo, B. A. Cervantes Vergara, A. E. Chavarria, E. Darragh-Ford, J. R. T. de Mello Neto, J. C. D’Olivo, J. Estrada, R. Gaïor, Y. Guardincerri, T. W. Hossbach, B. Kilminster, I. Lawson, S. J. Lee, A. Letessier-Selvon, A. Matalon, V. B. B. Mello, P. Mitra, J. Molina, S. Paul, A. Piers, P. Privitera, K. Ramanathan, J. Da Rocha, Y. Sarkis, M. Settimo, R. Smida, R. Thomas, J. Tiffenberg, D. Torres Machado, R. Vilar, and A. L. Virto (DAMIC Collaboration), *Phys. Rev. Lett.* **123**, 181802 (2019).
- [6] J. Tiffenberg, M. Sofu-Haro, A. Drlica-Wagner, R. Essig, Y. Guardincerri, S. Holland, T. Volansky, and T.-T. Yu, *Phys. Rev. Lett.* **119**, 131802 (2017).
- [7] D. Z. Freedman, *Phys. Rev. D* **9**, 1389 (1974).
- [8] R. Essig, J. Mardon, and T. Volansky, *Phys. Rev. D* **85**, 076007 (2012).
- [9] M. Crisler, R. Essig, J. Estrada, G. Fernandez, J. Tiffenberg, M. S. Haro, T. Volansky, and T.-T. Yu, *Physical review letters* **121**, 061803 (2018).
- [10] O. Abramoff, L. Barak, I. M. Bloch, L. Chaplinsky, M. Crisler, Dawa, A. Drlica-Wagner, R. Essig, J. Estrada, E. Etzion, G. Fernandez, D. Gift, M. Sofu-Haro, J. Taenzer, J. Tiffenberg, T. Volansky, and T.-T. Yu (SENSEI Collaboration), *Phys. Rev. Lett.* **122**, 161801 (2019).
- [11] L. Barak, I. M. Bloch, M. Cababie, G. Canelo, L. Chaplinsky, F. Chierchie, M. Crisler, A. Drlica-Wagner, R. Essig, J. Estrada, E. Etzion, G. F. Moroni, D. Gift, S. Munagavalasa, A. Orly, D. Rodrigues, A. Singal, M. S. Haro, L. Stefanazzi, J. Tiffenberg, S. Uemura, T. Volansky, and T.-T. Yu (SENSEI Collaboration), *Phys. Rev. Lett.* **125**, 171802 (2020).
- [12] G. Fernandez-Moroni, P. A. Machado, I. Martinez-Soler, Y. F. Perez-Gonzalez, D. Rodrigues, and S. Rosauro-Alcaraz, arXiv preprint arXiv:2009.10741 (2020).
- [13] N. Castelló-Mor, *Nuclear Instruments and Methods in Physics Research Section A: Accelerators, Spectrometers, Detectors and Associated Equipment* **958**, 162933 (2020), proceedings of the Vienna Conference on Instrumentation 2019.
- [14] “OSCURA dark matter experiment based on skipperccd technology,” <https://astro.fnal.gov/science/dark-matter/oscura/>.
- [15] S. E. Holland, D. E. Groom, N. P. Palaio, R. J. Stover, and M. Wei, *IEEE Transactions on Electron Devices* **50**, 225 (2003).
- [16] R. Widenhorn, M. M. Blouke, A. Weber, A. Rest, and E. Bodegom, in *Sensors and Camera Systems for Scientific, Industrial, and Digital Photography Applications III*, Vol. 4669, edited by N. Sampat, J. Canosa, M. M. Blouke, J. Canosa, and N. Sampat, International Society for Optics and Photonics (SPIE, 2002) pp. 193 – 201.
- [17] B. E. Burke and S. A. Gajar, *IEEE transactions on electron devices* **38**, 285 (1991).

- [18] P. Du, D. Egana-Ugrinovic, R. Essig, and M. Sholapurkar, arXiv preprint arXiv:2011.13939 (2020).
- [19] D. J. Bartelink, J. Moll, and N. Meyer, *Physical Review* **130**, 972 (1963).
- [20] A. Toriumi, M. Yoshimi, M. Iwase, Y. Akiyama, and K. Taniguchi, *IEEE Transactions on Electron Devices* **34**, 1501 (1987).
- [21] M. Lanzoni, E. Sangiorgi, C. Fiegna, M. Manfredi, and B. Ricco, *IEEE electron device letters* **12**, 341 (1991).
- [22] J. Bude, N. Sano, and A. Yoshii, *Physical Review B* **45**, 5848 (1992).
- [23] J. Tsang and J. Kash, *Applied Physics Letters* **70**, 889 (1997).
- [24] M. S. Haro, G. Cancelo, G. F. Moroni, X. Bertou, J. Tiffenberg, E. Paolini, and J. Estrada, in *2016 Argentine Conference of Micro-Nanoelectronics, Technology and Applications (CAMTA)* (IEEE, 2016) pp. 11–16.
- [25] M. Haro, G. Moroni, J. Tiffenberg, G. Cancelo, J. Estrada, X. Bertou, and E. Paolini, *Taking the CCDs to the ultimate performance for low threshold experiments*, Tech. Rep. (Fermi National Accelerator Lab.(FNAL), Batavia, IL (United States), 2016).